



HAL
open science

Passive wideband concentric rings resonator for vocal cords abnormalities detection: Application on larynx cancer pathologies

Sandrine Matta, Daher Diab, Nadine Saad, Dany Ishac, Georges Nassar

► To cite this version:

Sandrine Matta, Daher Diab, Nadine Saad, Dany Ishac, Georges Nassar. Passive wideband concentric rings resonator for vocal cords abnormalities detection: Application on larynx cancer pathologies. Review of Scientific Instruments, 2020, 91 (1), pp.015115. 10.1063/1.5090193 . hal-03322823

HAL Id: hal-03322823

<https://hal.science/hal-03322823>

Submitted on 2 Jun 2022

HAL is a multi-disciplinary open access archive for the deposit and dissemination of scientific research documents, whether they are published or not. The documents may come from teaching and research institutions in France or abroad, or from public or private research centers.

L'archive ouverte pluridisciplinaire **HAL**, est destinée au dépôt et à la diffusion de documents scientifiques de niveau recherche, publiés ou non, émanant des établissements d'enseignement et de recherche français ou étrangers, des laboratoires publics ou privés.

Passive wideband concentric rings resonator for vocal cords abnormalities detection: Application on larynx cancer pathologies

Cite as: Rev. Sci. Instrum. **91**, 015115 (2020); <https://doi.org/10.1063/1.5090193>

Submitted: 25 January 2019 • Accepted: 02 January 2020 • Published Online: 22 January 2020

 Sandrine Matta, Daher Diab,  Nadine Saad, et al.



View Online



Export Citation



CrossMark

ARTICLES YOU MAY BE INTERESTED IN

[An autonomous low-power management system for energy harvesting from a miniaturized spherical piezoelectric transducer](#)

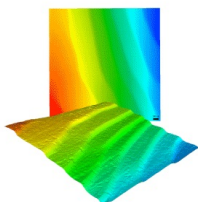
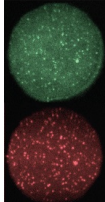
Review of Scientific Instruments **90**, 075004 (2019); <https://doi.org/10.1063/1.5084267>

[Development of a prototype radio-frequency system for a radio-frequency quadrupole cooler buncher in the rare isotope science project](#)

Review of Scientific Instruments **91**, 013324 (2020); <https://doi.org/10.1063/1.5128625>

[Upgrading the LANSCE accelerator with a SNS RF-driven \$H^-\$ ion source](#)

Review of Scientific Instruments **91**, 013321 (2020); <https://doi.org/10.1063/1.5129673>

 MCL MAD CITY LABS INC. www.madcitylabs.com	<p>Nanopositioning Systems</p> 	<p>Modular Motion Control</p> 	<p>AFM and NSOM Instruments</p> 	<p>Single Molecule Microscopes</p> 
---	--	--	---	--

Passive wideband concentric rings resonator for vocal cords abnormalities detection: Application on larynx cancer pathologies

Cite as: *Rev. Sci. Instrum.* **91**, 015115 (2020); doi: [10.1063/1.5090193](https://doi.org/10.1063/1.5090193)

Submitted: 25 January 2019 • Accepted: 2 January 2020 •

Published Online: 22 January 2020



View Online



Export Citation



CrossMark

Sandrine Matta,¹  Daher Diab,² Nadine Saad,³  Dany Ishac,¹  and Georges Nassar^{2,a} 

AFFILIATIONS

¹Department of Electrical Engineering, University of Balamand, Balamand, Lebanon

²Polytechnic University Hauts-de-France, Institute of Electronic, Microelectronics & Nanotechnology, IEMN, CNRS, UMR 8520, 59313 Valenciennes, France

³Department of Physics, Lebanese University, Fanar-Beirut, Lebanon

^aAuthor to whom correspondence should be addressed: gnassar@uphf.fr

ABSTRACT

This work addresses the study and design of a diagnostic device consisting of a thin-film sensor array based on 8-mm centered rings, acting as an autonomous acoustic sensor covering a wide range of resonance frequencies (0.1 KHz–2 MHz). In addition to its advantageous shape, this device integrates both the active vibratory element and the embedded electronics dedicated to coding, control, and analysis. The results show that the experimental device could be the basis of a telemedical platform for the objective assessment and monitoring of chronic laryngeal dysphonia through the spectro-temporal analysis of the vibration of the vocal cords. Furthermore, this non-invasive, non-intrusive protocol does not require the physical cooperation of the patient.

Published under license by AIP Publishing. <https://doi.org/10.1063/1.5090193>

I. INTRODUCTION

Oral communication is the major tool for human interactions, the vector of our identity, and the witness of our emotions. Some diseases might affect the vocal apparatus, which is the unit responsible of generating sounds in humans, thus leading to disabilities in oral communication. The most common encountered diseases in diagnosis are those related to the larynx and the vocal cords.¹⁻⁵

While some of these diseases are considered mild, affecting the individual for a short period of time, such as acute laryngitis, an inflammatory condition of the larynx which could cause a dysphonia, others might be more severe and serious, such as the laryngeal cancers that are mostly of a squamous cell carcinoma form. A large number of patients are diagnosed annually with laryngeal cancer, the latter being among the most common cancers of the upper aerodigestive tract. The treatment option for every individual depends on many factors, among which are the stage of the cancer and the location and size of the tumor, and the objective of that treatment

thus being either a cure of the disease or an extension of the survival years of the patient and his palliation. The most commonly used treatments might be of a single or combined modality of a radiation therapy, a surgery involving a partial or total laryngectomy, and chemotherapy. Other new types of treatments are still being developed and tested in clinical trials such as targeted therapy that uses drugs to attack specific cancer cells. However, regardless of the treatment care method, the chances of recovery from laryngeal cancer are still low, especially in the case of patients diagnosed in advanced and metastatic stages.⁶ From here, the importance of early detection of cancer arises, which might increase the patient's chance for a cure. This detection might be useful in the case of subjects showing early signs and symptoms of the disease including a sore throat and ear pain, as well as individuals having high risk factors such as heavy smokers, alcoholics, or those with a family history.

Nowadays, there exist several clinical methods for the screening and diagnosis of laryngeal cancer, requiring physical and/or surgical interventions such as laryngoscopy and endoscopy, both allowing a

biopsy; Computerized Tomography scan (CT scan); Magnetic Resonance Imaging (MRI); Positron Emission Tomography scan (PET scan), etc. On the other hand, research studies have been carried out recently to develop speech processing methods that can be used as a preliminary diagnosis of several voice pathologies. Most of these studies analyze sound in the audible bandwidth, which gives incomplete information on the vibratory state of the vocal cords, while some others worked on the improvement of existing techniques such as local imaging or scanning.⁷⁻¹¹

In this context, this work aims to evaluate some larynx physical property variations through a non-intrusive passive smart listening collar. The latter can provide systematic and *in vivo* screening for some laryngeal diseases, including laryngeal cancer, by spectro-temporal analysis of the voice signal resonance. This would allow the detection of these diseases at an early stage, even in people who still present no symptoms, which would permit early treatment and a higher chance of a cure.

The design of this diagnostic device requires a deep understanding of the media, such as multilayered biological tissues, in which the vocal cord vibrations propagate before reaching the surface of the neck. Therefore, in Sec. II, an analytical model is developed for this multilayered media, and the best position of the sensor is determined as well as its corresponding resonance frequency, based on the quality of the collected signal or extracted information (frequency). Based on the results, an appropriate sensor design is presented in Sec. III, and its resonance frequency is verified numerically and experimentally. In Sec. IV, the collar is used to carry a detailed examination on a significant number of individuals being either healthy or presenting some laryngeal disease. The collected data is analyzed and classified through a developed algorithm, allowing the building of a reference database which characterizes the frequency components of the voice signal produced by each case.

II. MECHANICAL MODEL OF THE MULTILAYERED TISSUES

A. Analytical approach

The study of the mechanical behavior of the tissues subject to the propagation of the wave generated by the vocal cord vibration is necessary in order to adapt the parameters of the receiving transducer for an optimum reception. In this context, the tissues surrounding the vocal folds are approximated to a fat layer in which the wave generated by vocal cord vibrations propagates before reaching the skin and then getting detected by the transducer. A coupling gel is placed on the individual's neck to allow a maximum transfer of the vibrations from the skin to the transducer. Figure 1 illustrates the corresponding layered model and the propagation of a plane wave in the structure. The fat layer modeled as a fluid is referred to as layer 0. The skin, labeled layer 1, is modeled as an elastic solid. The gel, referred to as layer 2, is modeled as a fluid with the same properties as the fat layer. The generated (incident) wave in layer 0, having amplitude I , propagates through layer 0 until it strikes the interface with the skin at $z = z_0$ with an incidence angle θ_0 . A percentage of this wave is reflected back in layer 0 with amplitude R , while the remaining part is transmitted into layer 1. This wave propagates through the skin layer until it strikes the interface between the skin and the

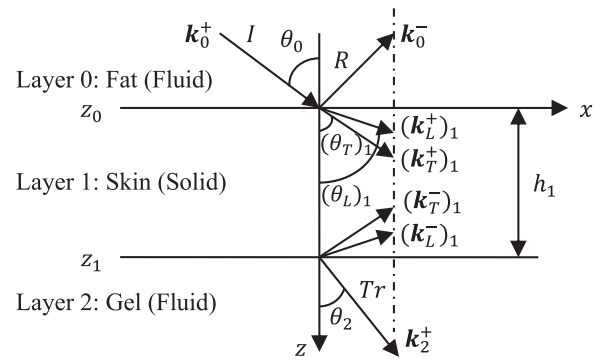


FIG. 1. A representation of the media through which the vocal cord vibrations propagate.

gel at $z = z_1$. Similarly, a percentage of that incident wave is reflected back in layer 1, while the remaining component is transmitted into the gel with amplitude Tr . The skin is a solid layer where two types of waves propagate: the longitudinal wave (denoted by the subscript L) and the shear or transverse wave (denoted by the subscript T). In this work, the stiffness matrix method¹² is implemented for an elastic solid layer bounded by two fluid semi-spaces, in order to model the wave propagation and compute the reflection and the transmission coefficients.

The displacement vector \mathbf{u}^m at any layer can be written as the summation of partial waves, where the number of partial waves (n) propagating in a medium depends on the nature or the type of the medium,¹¹

$$\mathbf{u}^m = \sum_{j=1}^n (a_j^+ \mathbf{p}_j^+ e^{ik_{zj}^+(z-z_{m-1})} + a_j^- \mathbf{p}_j^- e^{ik_{zj}^-(z-z_m)})_m e^{i(k_x x + k_y y - \omega t)}, \quad (1)$$

where $\mathbf{u}^m = [u_x^m, u_y^m, u_z^m]^T$, T refers to the transpose, j refers to the partial j th wave, and a_j^\pm refers to the j th displacement amplitude. The positive and negative superscripts refer to the wave propagated in the $(+z)$ and $(-z)$ directions, respectively. $\mathbf{p}_j^\pm (= [p_x^\pm, p_y^\pm, p_z^\pm]^T)$ represents the j th unit displacement polarization vector that corresponds to the j th partial wave with the wave vector $\mathbf{k}_j^\pm (= [k_x^\pm, k_y^\pm, k_z^\pm]^T)$. According to Snell's law, the x projection of the wave vector is equal for all propagating partial waves in all layers,

$$(k_{x,j})_m = k_x^0 = k_0 \sin \theta_0 = k_x \quad \forall j, m. \quad (2)$$

The coordinates system, as shown in Fig. 1, is chosen so that the (x, z) plane coincides with the incident plane and consequently, $k_y = 0$.

1. Fluid layer

The waves which are propagating in the fluid are only of the longitudinal type.¹² Therefore, two longitudinal waves propagate in the $(+z)$ and $(-z)$ directions. The wave number in the fluid is expressed as

$$k^+ = k^- = k = \frac{\omega}{c_f}, \quad (3)$$

where c_f is the speed of sound in the fluid. Then, $k_z^+ = -k_z^- = k \cos \theta$
 $= \sqrt{\frac{\omega^2}{(c_f)^2} - k_x^2}$.

The boundary conditions at the interface of a fluid layer express the continuity of the vertical displacement and the continuity of the fluid pressure.¹² Then, the displacement-stress column vector of the fluid layers (layer 0 and layer 2) is as follows:

$$U^m(x, z) = \begin{bmatrix} u_z \\ \sigma_{zz} \end{bmatrix}^m, \quad m = 0, 2. \quad (4)$$

The z component of the displacement vector is given by

$$u_z^m = (a^+ p_z^+ e^{ik_z^+(z-z_{m-1})} + a^- p_z^- e^{ik_z^-(z-z_m)})_m e^{i(k_x x - \omega t)}. \quad (5)$$

The unit displacement polarization vectors in the fluid are $\mathbf{p}_m^+ = [\sin \theta_m, 0, \cos \theta_m]^T$ and $\mathbf{p}_m^- = [\sin \theta_m, 0, -\cos \theta_m]^T$.

Moreover, the dilatation or pressure in the fluid can be defined as⁵

$$P = -\sigma_{zz} = -K_f \nabla \cdot \mathbf{u}, \quad (6)$$

where $K_f = (c_f)^2 \times \rho_f$ represents the bulk modulus of the fluid and ρ_f refers its density.

Taking the origin at $z = z_0$ for the upper half-space and at $z = z_1$ for the lower half-space and factorizing the displacement amplitudes a_m^\pm in the components of U^m , the latter vector can be expressed as

$$[U^m(x, z)] = [G^m][E^m(z)]A^m e^{i(k_x x - \omega t)}, \quad (7)$$

where $A^m = [a_m^+, a_m^-]^T$ is the amplitudes vector, $[E^m(z)]$ is a diagonal 2×2 matrix such that $diag\{[E^0(z)]\} = [e^{i(k_z^+)_0 z}, e^{i(k_z^-)_0 z}]$ and $diag\{[E^2(z)]\} = [e^{i(k_z^+)_2(z-z_1)}, e^{i(k_z^-)_2(z-z_1)}]$, and $[G^m]$ is a 2×2 matrix including the physical characteristics of the layer and hence called the layer characteristic matrix,

$$[G^m] = \begin{bmatrix} \cos \theta_m & -\cos \theta_m \\ i\omega K_f / c_f & i\omega K_f / c_f \end{bmatrix}. \quad (8)$$

2. Solid layer

Two types of waves can propagate in an isotropic elastic solid layer: the longitudinal wave (L wave) and the transverse or shear wave (T wave).¹³ The longitudinal and the transverse wave numbers are expressed as

$$(k_L^+)_1 = (k_L^-)_1 = (k_L)_1 = \frac{\omega}{c_L}, \quad c_L = \sqrt{\frac{\lambda + 2\mu}{\rho_s}}, \quad (9)$$

$$(k_T^+)_1 = (k_T^-)_1 = (k_T)_1 = \frac{\omega}{c_T}, \quad c_T = \sqrt{\frac{\mu}{\rho_s}},$$

where c_L and c_T are the speeds of the longitudinal and the transverse waves in the elastic solid, respectively. λ and μ are the Lamé coefficients of the solid, and ρ_s refers to its density. Then,

$$(k_{z,L}^+)_1 = -(k_{z,L}^-)_1 = \sqrt{(k_L)_1^2 - k_x^2} \quad (1)$$

and

$$(k_{z,T}^+)_1 = -(k_{z,T}^-)_1 = \sqrt{(k_T)_1^2 - k_x^2}. \quad (2)$$

The boundary conditions at the interface of a solid layer express the continuity of the x and z components of the displacement and the continuity of each of the tangential and the normal stresses. Then, the displacement-stress column vector of the solid layer (layer 1) is given by

$$U^1(x, z) = [u_x^1, u_z^1, \sigma_{xz}^1, \sigma_{zz}^1]^T. \quad (10)$$

The x and z components of the displacement vector can be expressed as follows:

$$u_x^1 = \sum_{j=L,T} (a_j^+ p_{xj}^+ e^{ik_{zj}^+(z-z_0)} + a_j^- p_{xj}^- e^{ik_{zj}^-(z-z_1)})_1 \times e^{i(k_x x - \omega t)} \quad (11)$$

and

$$u_z^1 = \sum_{j=L,T} (a_j^+ p_{zj}^+ e^{ik_{zj}^+(z-z_0)} + a_j^- p_{zj}^- e^{ik_{zj}^-(z-z_1)})_1 \times e^{i(k_x x - \omega t)}, \quad (12)$$

where

$$(\mathbf{p}_L^+)_1 = [\sin(\theta_L)_1, 0, \cos(\theta_L)_1]^T,$$

$$(\mathbf{p}_L^-)_1 = [\sin(\theta_L)_1, 0, -\cos(\theta_L)_1]^T,$$

$$(\mathbf{p}_T^+)_1 = [-\cos(\theta_T)_1, 0, \sin(\theta_T)_1]^T,$$

$$(\mathbf{p}_T^-)_1 = [\cos(\theta_T)_1, 0, \sin(\theta_T)_1]^T. \quad (3)$$

The two angles $(\theta_L)_1$ and $(\theta_T)_1$ are the angles relative to the longitudinal and shear waves, respectively.

The stress-strain tensor for an elastic solid is defined as

$$\sigma_{rs} = 2\mu \varepsilon_{rs} + \delta_{rs} \lambda \nabla \cdot \mathbf{u}, \quad r, s = x, y, z, \quad (13)$$

where δ_{rs} is the Kronecker delta, $\delta_{rs} = \begin{cases} 1, & r = s \\ 0, & r \neq s \end{cases}$, and ε_{rs} is the strain tensor defined as $\varepsilon_{rs} = \frac{1}{2} (\frac{\partial u_r}{\partial s} + \frac{\partial u_s}{\partial r})$.

Factorizing the displacement's amplitudes $(a_{L,T}^\pm)_1$ in the components of U^1 , the latter vector can be expressed as

$$[U^1(x, z)] = [G^1][E^1(z)]A^1 e^{i(k_x x - \omega t)}, \quad (14)$$

where $A^1 = [(a_L^+)_1, (a_L^-)_1, (a_T^+)_1, (a_T^-)_1]^T$ is the amplitudes vector, $[E^1(z)]$ is a diagonal 4×4 matrix such that $diag\{[E^1(z)]\} = [e^{i(k_{z,L}^+)_1(z-z_0)}, e^{i(k_{z,L}^-)_1(z-z_0)}, e^{i(k_{z,T}^+)_1(z-z_1)}, e^{i(k_{z,T}^-)_1(z-z_1)}]$, and the 4×4 characteristic matrix for the solid is reduced to

$$[\mathbf{G}^1] = \begin{bmatrix} \sin(\theta_L)_1 & -\cos(\theta_T)_1 & \sin(\theta_L)_1 & \cos(\theta_T)_1 \\ \cos(\theta_L)_1 & \sin(\theta_T)_1 & -\cos(\theta_L)_1 & \sin(\theta_T)_1 \\ \frac{j\mu\omega}{c_L} \sin 2(\theta_L)_1 & -\frac{j\mu\omega}{c_T} \cos 2(\theta_T)_1 & -\frac{j\mu\omega}{c_L} \sin 2(\theta_L)_1 & -\frac{j\mu\omega}{c_T} \cos 2(\theta_T)_1 \\ \frac{j2\mu\omega}{c_L} (\cos(\theta_L)_1)^2 + \frac{j\lambda\omega}{c_L} & \frac{j\mu\omega}{c_T} \sin 2(\theta_T)_1 & \frac{j2\mu\omega}{c_L} (\cos(\theta_L)_1)^2 + \frac{j\lambda\omega}{c_L} & -\frac{j\mu\omega}{c_T} \sin 2(\theta_T)_1 \end{bmatrix}. \quad (15)$$

The total displacement in layer 1 at the upper interface ($z = z_0$) and the lower interface ($z = z_1$) can be expressed as

$$\mathbf{u}^1(x, z_0) = e^{i(k_x x - \omega t)} \left(\sum_{j=L,T} (a_j^+ \mathbf{p}_j^+) \Big|_1 + \sum_{j=L,T} (a_j^- \mathbf{p}_j^- e^{-ik_{z_j}^- h_1}) \Big|_1 \right), \quad (16)$$

$$\mathbf{u}^1(x, z_1) = e^{i(k_x x - \omega t)} \left(\sum_{j=L,T} (a_j^+ \mathbf{p}_j^+ e^{ik_{z_j}^+ h_1}) \Big|_1 + \sum_{j=L,T} (a_j^- \mathbf{p}_j^-) \Big|_1 \right),$$

where $h_1 = z_1 - z_0$ is the thickness of the layer 1. Since $(k_{z_j}^+) \Big|_1 = -(k_{z_j}^-) \Big|_1$, then $e^{-i(k_{z_j}^-) \Big|_1 h_1} = e^{i(k_{z_j}^+) \Big|_1 h_1}$.

The vector \mathbf{u}^1 is of size two including its x and z components ($\mathbf{u}^1 = [u_x^1, u_z^1]^T$). If the characteristic matrix $[\mathbf{G}^1]$ in Eq. (15) is subdivided into four equal 2×2 submatrices, $[\mathbf{G}_1] = \begin{bmatrix} [\mathbf{G}_{11}^1] & [\mathbf{G}_{12}^1] \\ [\mathbf{G}_{21}^1] & [\mathbf{G}_{22}^1] \end{bmatrix}$, the elements in Eq. (16) can be written in the matrix form as follows:

$$\begin{bmatrix} \mathbf{u}^1(x, z_0) \\ \mathbf{u}^1(x, z_1) \end{bmatrix} = \begin{bmatrix} [\mathbf{G}_{11}^1] & [\mathbf{G}_{12}^1][\mathbf{H}^1] \\ [\mathbf{G}_{21}^1][\mathbf{H}^1] & [\mathbf{G}_{22}^1] \end{bmatrix} \mathbf{A}^1 e^{i(k_x x - \omega t)}$$

$$= [\mathbf{E}_u^1] \mathbf{A}^1 e^{i(k_x x - \omega t)}, \quad (17)$$

where $[\mathbf{H}^1]$ is a square diagonal matrix whose elements are $\text{diag}\{[\mathbf{H}^1]\} = e^{i(k_{z_j}^+) \Big|_1 h_1}$.

Similarly, the stresses in layer 1 at the upper interface ($z = z_0$) and the lower interface ($z = z_1$) can be expressed as

$$\begin{bmatrix} \boldsymbol{\sigma}^1(x, z_0) \\ \boldsymbol{\sigma}^1(x, z_1) \end{bmatrix} = \begin{bmatrix} [\mathbf{G}_{21}^1] & [\mathbf{G}_{22}^1][\mathbf{H}^1] \\ [\mathbf{G}_{11}^1][\mathbf{H}^1] & [\mathbf{G}_{12}^1] \end{bmatrix} \mathbf{A}^1 e^{i(k_x x - \omega t)}$$

$$= [\mathbf{E}_\sigma^1] \mathbf{A}^1 e^{i(k_x x - \omega t)}, \quad (18)$$

where $\boldsymbol{\sigma}^1 = [\sigma_{xz}^1, \sigma_{zz}^1]^T$. By substituting the amplitudes vector from Eq. (17) into Eq. (18), the stresses and the displacements will be related through the layer's stiffness matrix $[\mathbf{K}^1]$ or the compliance matrix $[\mathbf{S}^1]$ as follows:

$$\begin{bmatrix} \boldsymbol{\sigma}^1(x, z_0) \\ \boldsymbol{\sigma}^1(x, z_1) \end{bmatrix} = [\mathbf{E}_\sigma^1][\mathbf{E}_u^1]^{-1} \begin{bmatrix} \mathbf{u}^1(x, z_0) \\ \mathbf{u}^1(x, z_1) \end{bmatrix} = [\mathbf{K}^1] \begin{bmatrix} \mathbf{u}^1(x, z_0) \\ \mathbf{u}^1(x, z_1) \end{bmatrix},$$

$$\begin{bmatrix} \mathbf{u}^1(x, z_0) \\ \mathbf{u}^1(x, z_1) \end{bmatrix} = [\mathbf{E}_u^1][\mathbf{E}_\sigma^1]^{-1} \begin{bmatrix} \boldsymbol{\sigma}^1(x, z_0) \\ \boldsymbol{\sigma}^1(x, z_1) \end{bmatrix} = [\mathbf{S}^1] \begin{bmatrix} \boldsymbol{\sigma}^1(x, z_0) \\ \boldsymbol{\sigma}^1(x, z_1) \end{bmatrix}, \quad (19)$$

$$[\mathbf{S}^1] = [\mathbf{K}^1]^{-1}.$$

3. Fluid-Solid interface

The boundary conditions at a fluid-solid interface are expressed at the first interface ($z = z_0$) as

$$\begin{cases} u_z^0(z_0) = u_z^1(z_0), \\ \sigma_{zz}^0(z_0) = \sigma_{zz}^1(z_0), \\ \sigma_{xz}^1(z_0) = 0. \end{cases} \quad (20)$$

The same conditions apply to the second interface ($z = z_1$),

$$\begin{cases} u_z^1(z_1) = u_z^2(z_1), \\ \sigma_{zz}^1(z_1) = \sigma_{zz}^2(z_1), \\ \sigma_{xz}^1(z_2) = 0. \end{cases} \quad (21)$$

4. Reflection and transmission coefficients

The reflection coefficient (R) in the incidence medium and the transmission coefficient (Tr) in the transmission medium are obtained for a unity incident plane wave ($I = 1$), in function of the incidence angle θ_0 and the frequency of the incident wave. It is to be noted here that the refracted angles are related, according to Snell's law,¹⁴ as follows:

$$\frac{\sin \theta_0}{c_f} = \frac{\sin(\theta_T)_1}{c_T} = \frac{\sin(\theta_L)_1}{c_L} = \frac{\sin \theta_2}{c_f}. \quad (22)$$

Since layer 0 and layer 2 are identical, $\theta_0 = \theta_2$ and they have the same characteristic matrix ($[\mathbf{G}^0] = [\mathbf{G}^2]$).

It is to be noted that the term $e^{i(k_x x - \omega t)}$ is omitted in the following expressions since it will be canceled in the calculations.

In the incidence medium, expressing Eq. (7) at $z = z_0$ with $\mathbf{A}^0 = [1, R]^T$ yields

$$\begin{cases} u_z^0(z_0) = G_{11}^0 + R G_{12}^0, \\ \sigma_{zz}^0(z_0) = G_{21}^0 + R G_{22}^0. \end{cases} \quad (23)$$

G_{ab}^0 is the component of the a th row and b th column of the fluid medium's characteristic matrix.

Since layer 2 is the last layer, there is no reflection (i.e., $a_2^- = 0$). Then, by expressing similarly Eq. (7) in the transmission medium at $z = z_1$ and with $\mathbf{A}^2 = [Tr, 0]^T$, the following is obtained:

$$\begin{cases} u_z^2(z_1) = Tr G_{11}^2, \\ \sigma_{zz}^2(z_1) = Tr G_{21}^2. \end{cases} \quad (24)$$

Now, by relating the displacements and the stresses in layer 1 at its top and bottom surfaces by the compliance matrix as defined in

Eq. (19) and by using the boundary conditions defined in Eqs. (20) and (21), the following system of equations can be obtained:

$$\begin{cases} u_z^0(z_0) = S_{22}^1 \sigma_{zz}^0(z_0) + S_{24}^1 \sigma_{zz}^2(z_1), \\ u_z^2(z_1) = S_{42}^1 \sigma_{zz}^0(z_0) + S_{44}^1 \sigma_{zz}^2(z_1). \end{cases} \quad (25)$$

By substituting Eqs. (23) and (24) in Eq. (25) and solving for R and Tr , the following is obtained:

$$\begin{bmatrix} R \\ Tr \end{bmatrix} = \begin{bmatrix} G_{12}^0 - S_{22}^1 G_{22}^0 - S_{24}^1 G_{21}^2 \\ -S_{42}^1 G_{22}^0 G_{11}^2 - S_{44}^1 G_{21}^2 \end{bmatrix}^{-1} \begin{bmatrix} S_{22}^1 G_{21}^0 - G_{11}^0 \\ S_{42}^1 G_{21}^0 \end{bmatrix}. \quad (26)$$

B. Results and analysis

The transmitted wave in the transmission medium (gel) is acquired by the transducer attached to the individual's neck using a collar. The position of the transducer may greatly affect the collected signal and consequently the results for identification and classification purposes in the medical application. The position of the transducer can be defined in terms of the angle (θ_2), the angle made with the normal to the longitudinal axis (z -axis). In order to examine the best location, the transmission coefficient is obtained, as outlined earlier, as a function of the incident plane wave incidence angle θ_0 and frequency. The best incident angle θ_0 is the angle that yields the highest transmission coefficient for all frequencies. The physical parameters of the media simulating the model are outlined in Table I.^{15,16} The incident angle θ_0 varies from 0° to 90° with an increment of 1° . Similarly, the frequency of the generated signal varies from 0 KHz to 2 KHz with an increment of 1 Hz since it can be seen clearly in the literature that there are no frequency contents above 2 KHz detected by a contact microphone.¹⁷

In Fig. 2, the magnitude of the reflection coefficient is represented as a function of the variations of the frequency f and incidence angle θ_0 in a two-dimensional mapping diagram, with a gray level scaled from zero to one corresponding, respectively, to a maximum transmission ($R = 0$) and a total reflection ($Tr = 0$). The diagram shows that there is practically a good transmission for almost all the incidence angles. However, if the incidence angle is between 70° and 90° , the transmission is low for high frequencies. In other words, the frequencies that are above 300 Hz might be altered or even not received. Moreover, there is no transmission of the incident signal if the incident angle is between 87° and 90° for the range of frequencies. Therefore, it is not recommended to attach a transducer inside the region that corresponds to the interval $[70^\circ-90^\circ]$. The highest transmission coefficients which are observed correspond to an incident angle in the range of $[0^\circ-70^\circ]$. This can be referred to as the safe region to attach the transducer.

TABLE I. Physical parameters of the fluid and solid layers.

Fluid	Density (ρ_f)	920 Kg m ⁻³
	Speed of sound in fluid (c_f)	1450 m s ⁻¹
Solid	Thickness (h)	2 mm
	Density (ρ_s)	1050 Kg m ⁻³
	μ	2.1 Mpa
	λ	50.4 Mpa

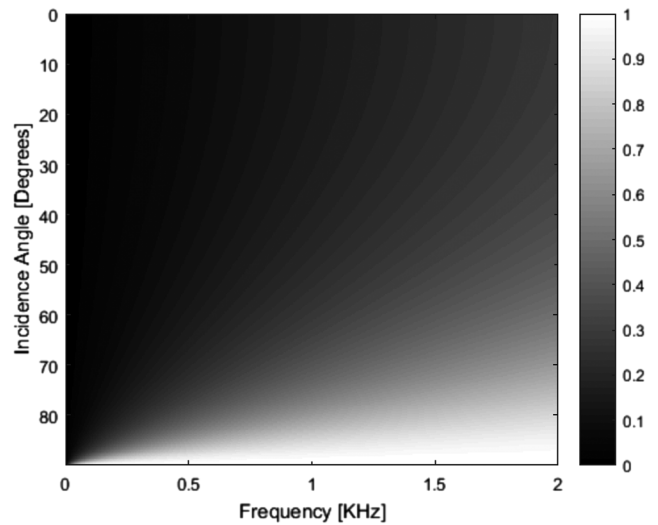


FIG. 2. Magnitude of the reflection coefficient as a function of $[f, \theta]$ for the simulated model (fluid-solid-fluid).

III. LOW FREQUENCY MICRO-RESONATOR DESIGN

The numerical results of Sec. III give the suitable position where the sensor should be attached on the collar with respect to the human neck and the corresponding frequency for an optimum reception of the information. Since the operation of the sensor is expected at a low-frequency (below 2 kHz band) and knowing that the resonance frequency of a resonant piezoelectric transducer vibrating in a thickness mode is inversely proportional to its size, the main challenge here is to design and build an acoustic receiver being able to operate at a low-frequency but at the same time of a miniature size.

In this context, a transducer is designed based on the concept of resonant concentric thin rings of reduced size rather than the classic sensor design. The physical parameters of the receptors are chosen in accordance with the results (Fig. 3) obtained from a simulation study by the ANSYS[®] software (ANSYS Academic Research Mechanical, Release 10, Coupled Field Analysis, ANSYS, Inc.), consolidated by the mechanical analytical model (Fig. 4) while taking into account the physical and electromechanical properties of the piezo-elements used. The transducer is built then according to the design parameters, and the results are validated experimentally.

A. Mechanical approach

In order to validate the approach, the mechanical behavior is assessed and the study is completed by a numerical simulation based on the application of the finite element method to characterize the resonator vibration modes and visualize the corresponding distortions when the structure is excited. This concordance gives access to set in practice the experimental element to receive waves coupled by tissues and validates the findings.

From a mechanical point of view, the dynamics of the system are expressed by the following differential equations:

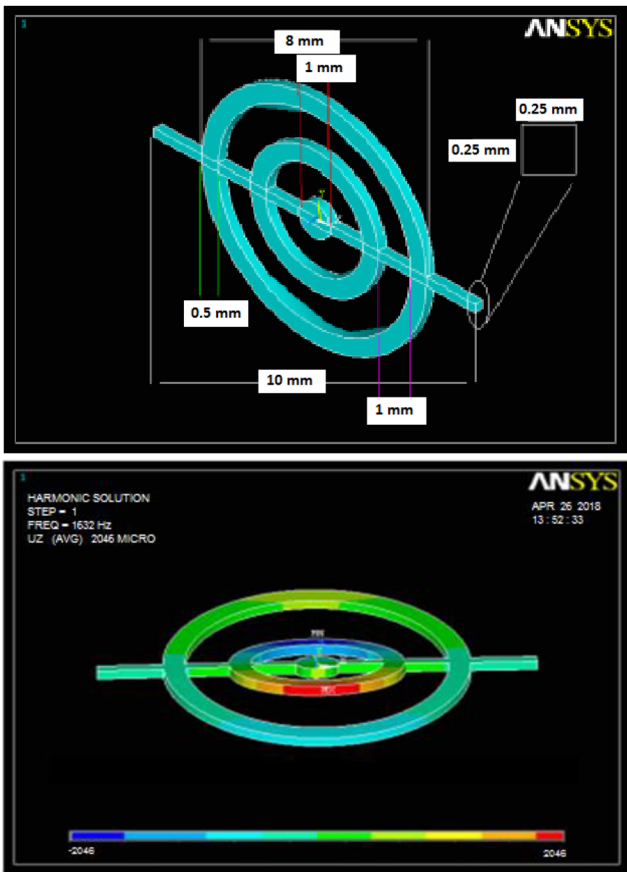


FIG. 3. Geometrical dimensions and modular resonance ($f = 1.632$ kHz) of the concentric ring sensor.

- Mass m_1 :

$$m_1 \ddot{x}_1 + k_1 x_1 + k_2(x_1 - x_2) + c_1 \dot{x}_1 + c_2(\dot{x}_1 - \dot{x}_2) = 0$$

$$\Rightarrow \ddot{x}_1 + \Omega_1^2 x_1 + \Delta_1 \dot{x}_1 - \frac{k_2}{m_1} x_2 - \frac{c_2}{m_1} \dot{x}_2 = 0, \quad (27)$$

where $\Omega_1^2 = \frac{k_1+k_2}{m_1}$ and $\Delta_1 = \frac{c_1+c_2}{m_1}$.

- Mass m_2 :

$$m_2 \ddot{x}_2 + k_2(x_2 - x_1) + k_3(x_2 - x_3) + c_2(\dot{x}_2 - \dot{x}_1) + c_3(\dot{x}_2 - \dot{x}_3) = 0$$

$$\Rightarrow \ddot{x}_2 + \Omega_2^2 x_2 + \Delta_2 \dot{x}_2 - \frac{k_2}{m_2} x_1 - \frac{c_2}{m_2} \dot{x}_1 - \frac{k_3}{m_2} x_3 - \frac{c_3}{m_2} \dot{x}_3 = 0, \quad (28)$$

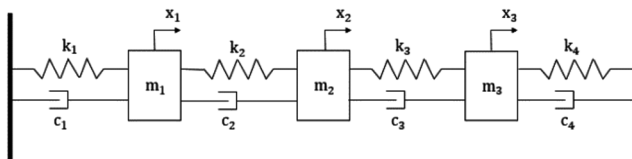


FIG. 4. Mechanical equivalent model of the sensor, where k and c reflect the spring and dashpot characteristics.

where $\Omega_2^2 = \frac{k_2+k_3}{m_2}$ and $\Delta_1 = \frac{c_2+c_3}{m_2}$.

- Mass m_3 :

$$m_3 \ddot{x}_3 + k_4 x_3 + k_3(x_3 - x_2) + c_4 \dot{x}_3 + c_3(\dot{x}_3 - \dot{x}_2) = 0$$

$$\Rightarrow \ddot{x}_3 + \Omega_3^2 x_3 + \Delta_3 \dot{x}_3 - \frac{k_3}{m_3} x_2 - \frac{c_3}{m_3} \dot{x}_2 = 0, \quad (29)$$

where $\Omega_3^2 = \frac{k_3+k_4}{m_3}$ and $\Delta_3 = \frac{c_3+c_4}{m_3}$.

Grouping the three differential equations in Eqs. (27)–(29) for the three masses leads to the following system of equations:

$$\begin{cases} \ddot{x}_1 + \Omega_1^2 x_1 + \Delta_1 \dot{x}_1 - \frac{k_2}{m_1} x_2 - \frac{c_2}{m_1} \dot{x}_2 = 0, \\ \ddot{x}_2 + \Omega_2^2 x_2 + \Delta_2 \dot{x}_2 - \frac{k_2}{m_2} x_1 - \frac{c_2}{m_2} \dot{x}_1 - \frac{k_3}{m_2} x_3 - \frac{c_3}{m_2} \dot{x}_3 = 0, \\ \ddot{x}_3 + \Omega_3^2 x_3 + \Delta_3 \dot{x}_3 - \frac{k_3}{m_3} x_2 - \frac{c_3}{m_3} \dot{x}_2 = 0. \end{cases} \quad (30)$$

A sinusoidal motion with ω as pulsation leads to express the following displacement system:

$$\begin{cases} x_1 = A e^{i\omega t}, \\ x_2 = B e^{i\omega t}, \\ x_3 = D e^{i\omega t}. \end{cases}$$

Considering the expressions of x_i ($i = 1, 2, 3$) and their derivations, the system of equations yields

$$\begin{cases} (\Omega_1^2 - \omega^2 + j\omega\Delta_1)A - \left(\frac{K}{m_1} + \frac{j\omega c}{m_1}\right)B = 0, \\ -\left(\frac{K}{m_2} + \frac{j\omega c}{m_2}\right)A + (\Omega_2^2 - \omega^2 + j\omega\Delta_2)B - \left(\frac{K}{m_2} + \frac{j\omega c}{m_2}\right)D = 0, \\ -\left(\frac{K}{m_3} + \frac{j\omega c}{m_3}\right)B + (\Omega_3^2 - \omega^2 + j\omega\Delta_3)D = 0, \end{cases} \quad (31)$$

with $k_1 = k_2 = k_3 = k_4$ and $c_1 = c_2 = c_3 = c_4$.

For there to be a non-zero solution, the determinant must be zero,

$$\begin{vmatrix} \Omega_1^2 - \omega^2 + j\omega\Delta_1 & -\left(\frac{K}{m_1} + \frac{j\omega c}{m_1}\right) & 0 \\ -\left(\frac{K}{m_2} + \frac{j\omega c}{m_2}\right) & (\Omega_2^2 - \omega^2 + j\omega\Delta_2) & -\left(\frac{K}{m_2} + \frac{j\omega c}{m_2}\right) \\ 0 & -\left(\frac{K}{m_3} + \frac{j\omega c}{m_3}\right) & (\Omega_3^2 - \omega^2 + j\omega\Delta_3) \end{vmatrix} = 0. \quad (32)$$

Applying the following numerical values,

- $k = 2.102$ N/m,
- $c = 0.2$,
- $m_1 = 4835 \times 10^{-6}$ Kg,
- $m_2 = 1088 \times 10^{-8}$ Kg, and
- $m_3 = 1813 \times 10^{-8}$ Kg,

the solutions of the following differential equation:

$$-\omega^6 + 5,9.107 j\omega^5 + 6,2.1014\omega^4 - 3,15.1019 j\omega^3 - 1.1023\omega^2 + 1.1026j\omega + 3,4.1028 = 0, \quad (33)$$

gives resonance frequency values at $f_0 = 1.6$ kHz, $f_1 = 85.3$ kHz, and $f_2 = 2.1$ MHz.

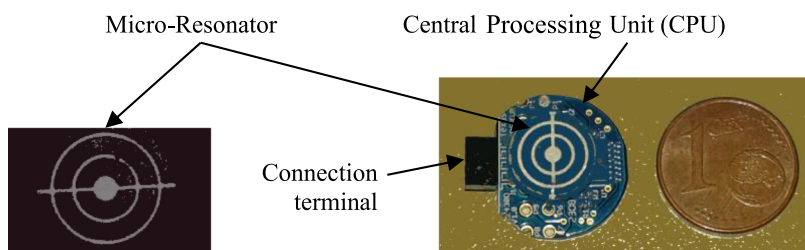


FIG. 5. Physical concept of the micro-resonator acoustic system.

TABLE II. Comparison of the resonance frequencies obtained from the numerical simulation, the mechanical model, and the experimental results.

Frequencies (kHz)	ANSYS 10	Mechanical model	Experimental results
f_0	1.63	1.6	1.53
f_1	85	85.3	84.6
f_2	2310	2100	1980

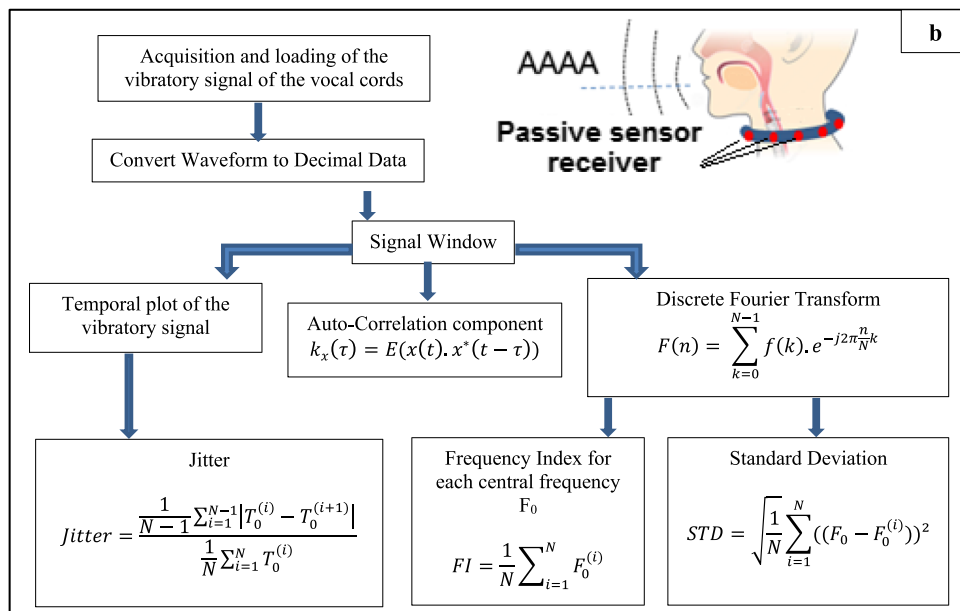
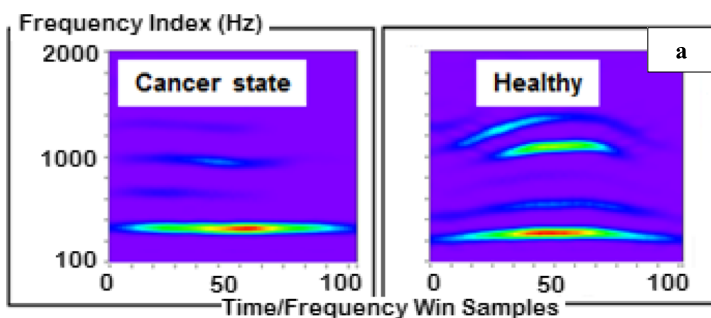


FIG. 6. (a) Spectrograms showing the different frequency components weights for two extreme physiological states: a healthy case and a cancerous state. (b) Sensor position and algorithm steps used for the classification of the different pathological states of the larynx.

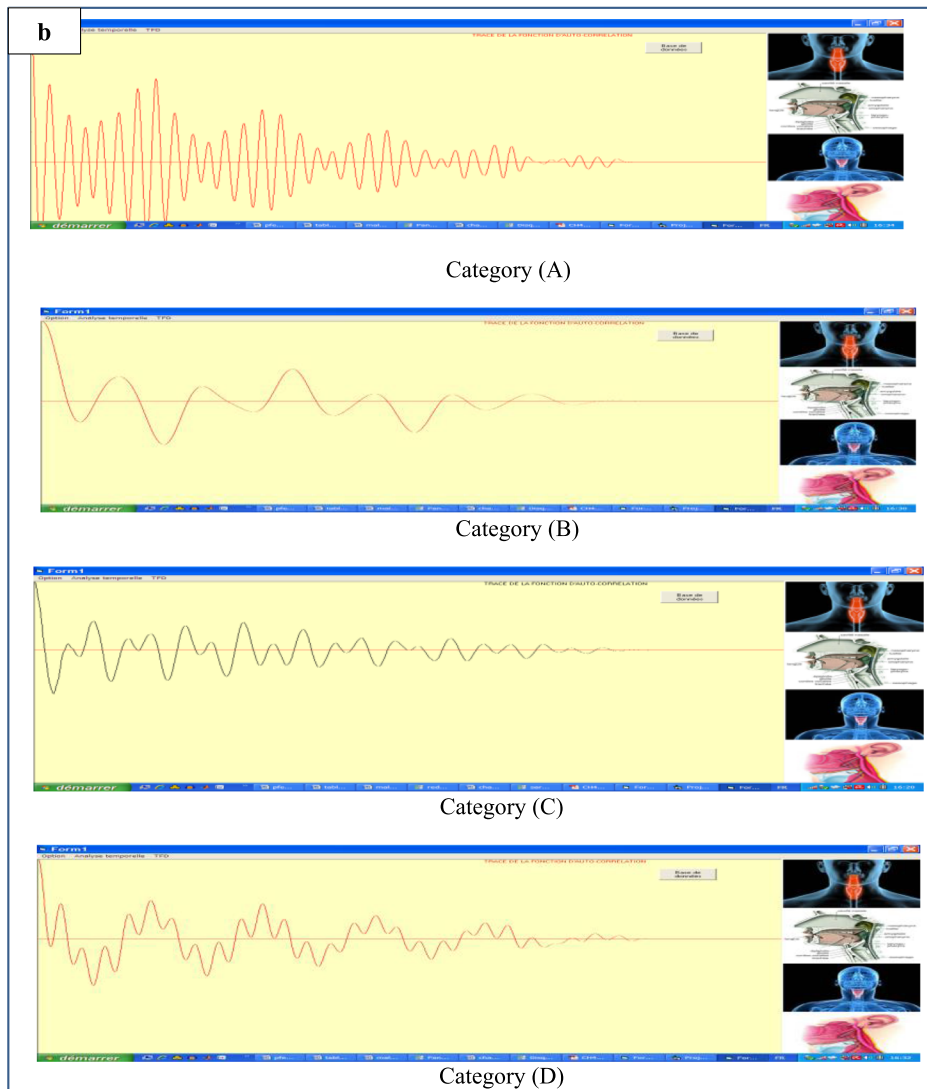
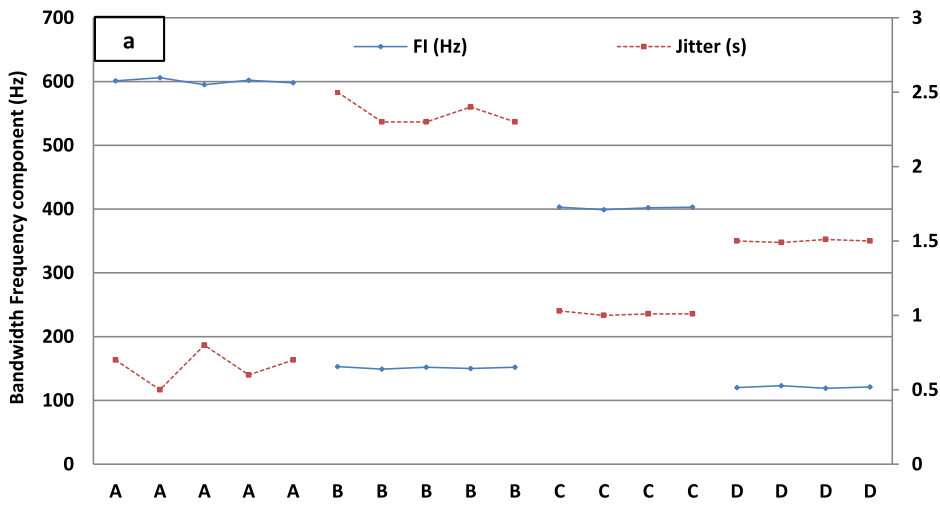


FIG. 7. (a) Classification resulting from the coupling of data from frequency components with those from the Jitter thus shows four distinct physiological states: (A) healthy patients, (B) cancer state, (C) inflammatory polypus, and (D) chronic laryngitis. (b) Graphical interface of the connected system showing the morphological diagram of the signal issued from each category.

B. Experimental realization of the sensor

The experimental realization of the receiver is elaborated on the basis of a piezoelectric disk of diameter at the base of 10 mm and a thickness of 0.25 mm (PZ26 Ferroperm). The central concentric rings are made through an assisted laser engraving system. Other than the physical maintenance of the rings, the central rod allows both electrical polarization and electrical continuity with the central control unit (Fig. 5).

Table II shows a good agreement between the main resonance frequency values obtained from the numerical simulation, the analytical model, and the experimental response by a network analyzer. These results ensure that the designed transducer has a fundamental resonance frequency (around 1.6 Hz) which makes it convenient to be used in this medical application.

IV. *IN VIVO* DISEASES DETECTION

Having succeeded to design a miniature sensor with a low resonance frequency and having found the suitable position where it should be attached on the collar to be wrapped around the human neck for an optimum information reception, the collar is implemented and is used to carry a detailed examination on four different categories of people: healthy cases, subjects with laryngeal cancer, those suffering from inflammatory polypus, and the ones having chronic laryngitis. Figure 6(a) shows the spectrograms of the two extreme physiological cases: a healthy state vs a cancerous one. In our application, 100 patients with an average age of 53 years of whom 20% were women were diagnosed in the same context but separately. The vibratory signal was acquired after each person pronounced the vowel /a/ [Fig. 6(b)], which reflects the greatest number of vocal cord vibration modes.^{18,19} For each person, an average of three signals was recorded in order to avoid the natural dispersion resulting from the experimental application.

The detected signals are treated using an algorithm based on the short time/frequency transform coupled with the Jitter index for each frequency band on the time signal, the steps of the algorithm being detailed in Fig. 6(b). A feature vector for each individual is stored in the database (training set), and the remaining acquired feature vectors (or signals) are used to study the performance of the system. A very high recognition rate has been achieved (above 90%).

In order to validate the concept experimentally, the hundreds of cases concerned were classified under 4 categories (20 subjects by category):

Category A for healthy subjects

Category B for subjects with laryngitis cancer

Category C relates to inflammatory polyp disease

Category D reflects chronic inflammation.

To reduce intra-category dispersion, 4 subgroups (5 subjects by group) were identified by setting a cross-correlation coefficient threshold between the time signals that are derived from subjects belonging to each category.

Figure 7(a) shows that the fundamental frequency of the waves produced by the vibration of the vocal cords in healthy subjects (A) is around 600 Hz with a standard deviation (STD) of 13 Hz. The Jitter,

which represents the characteristic temporal index of the sound, is located at around 0.7.

For subjects with larynx cancer (B), this frequency index is around 150 Hz (STD = 5 Hz) and the Jitter value is considerably higher at around 2.5.

In addition, for patients with benign lesions (C) of the larynx (vocal cord polyps), the fundamental frequency is around 400 Hz (STD = 8 Hz) and the Jitter is around 1.1, whereas for patients with chronic laryngitis (D), the fundamental frequency is around 110 Hz (STD = 4 Hz) and the Jitter is around 1.5.

In what follows, Fig. 7(b) gives an idea about the display of data and the classification of categories in a real environment. It shows an example of the graphical interface implemented providing the time signature of the signals for each of the above-mentioned patient categories.

The ENT examination shows that in a healthy subject, the laryngeal pathway is normal with good mobility of the vocal cords (A). The envelope of the autocorrelation function (of the time signal) is a sinc function; it is maximal at the intercept and contains several secondary periodic lobes resulting from the periodicity of the vibration of the vocal cords.

For a person with cancer (B), the temporal plot is irregular (random) and the spectrum is limited to low frequencies due to a significant decrease in and even total absence of vibration of the vocal cords.

As for subjects with inflammatory polyps or chronic laryngitis (C and D), the temporal plot contains some irregularities but also shows some similarities with the temporal plot of healthy patients. Additionally, the spectrum contains high frequencies but with lower values than healthy subjects.

V. CONCLUSIONS

In this paper, a non-invasive method is proposed for screening pathological states of human larynx. It consists of attaching a smart collar on the human neck where a transducer is attached to detect the wave generated by the vocal cord vibrations when the individuals pronounce the vowel /a/. A study has been done first to model that wave propagation and decide about the best location of the transducer with respect to the human neck, as well as the corresponding resonance frequency of the transducer for an optimum information reception. Based on that, a micro-transducer based on the concept of resonant concentric thin rings has been designed and built.

The collar has then been used for medical diagnosis of a given sample of individuals presenting different laryngeal pathological states. The acquired signals have been treated according to a developed algorithm, and a corresponding database has been built to classify the frequency components of every pathological case. An experimental result has shown the validity of the proposed idea with a rate of classification accuracy of about 90%. The 10% dispersal in overall diagnosis is related in part to the acute frequency component of the female sex. Work is underway to develop a characteristic chart for each sex to minimize this dispersion and make the system more reliable.

As a result, this work presents a “soft” and reliable diagnostic system based on the vibratory mechanical behavior of the vocal apparatus. A double interest results in the prospects of such an application:

1. Clinically, this system has been studied and designed to implement an alternative screening method for laryngeal pathologies to save patients from frequent exposure to harmful radiation as RX, MRI, etc.
2. In terms of prevention, the connected feature of this system offers a means of continuous information on the evolution of a state of health, continuously viewable by a “smart phone” interface, which could lead to possible early detection of severe laryngeal diseases, especially cancer, giving the subject a higher chance of cure.

REFERENCES

- ¹K. Omori, “Diagnosis of voice disorders,” *Jpn. Med. Assoc. J.* **54**, 248 (2011).
- ²D. D. Mehta and R. E. Hillman, *Curr. Opin. Otolaryngol. Head Neck Surg.* **20**(6), 429 (2012).
- ³F. Chen, S. Li, Y. Zhang, and J. Wang, “Benzothiazole-based fluorescent sensor for hypochlorite detection and its application for biological imaging,” *Sensors* **17**(3), 543 (2017).
- ⁴M. T. Turan and E. Erzin, *IEEE/ACM Trans. Audio, Speech, Lang. Process.* **24**(2), 265 (2016).
- ⁵A. Castellana, A. Carullo, S. Corbellini, A. Astolfi, M. S. Bisetti, and J. Colombini, “Cepstral peak prominence smoothed distribution as discriminator of vocal health in sustained vowel,” in *IEEE—Instrumentation and Measurement Technology Conference (I2MTC)* (IEEE, 2017), pp. 1–6.
- ⁶K. A. Gold, H.-Y. Lee, and E. S. Kim, “Targeted therapies in squamous cell carcinoma of the head and neck,” *Cancer* **115**(5), 922–935 (2009).
- ⁷M. R. Kaushik, A. S. Kole, N. Gupta, S. Dhoot, and A. Dehadaray, “Evaluation of various laryngeal pathologies: Videolaryngoscopy versus videolaryngostroboscopy,” *Indian J. Otolaryngol. Head Neck Surg.* **70**(2), 244–248 (2018).
- ⁸A. Ben Aicha and K. Ezzine, “Cancer larynx detection using glottal flow parameters and statistical tools,” in 2016 International Symposium on Signal, Image, Video and Communications (ISIVC), 2016.
- ⁹H. Cordeiro and C. Meneses, “Low band continuous speech system for voice pathologies identification,” in 2018 Signal Processing: Algorithms, Architectures, Arrangements, and Applications (SPA), 2018.
- ¹⁰A. Ben Aicha, “Noninvasive detection of potentially precancerous lesions of vocal fold based on glottal wave signal and SVM approaches,” *Proc. Comput. Sci.* **126**, 586–595 (2018).
- ¹¹S. Hegde, S. Shetty, S. Rai, and T. Dodderi, “A survey on machine learning approaches for automatic detection of voice disorders,” *J. Voice* **33**, 947.e11–947.e33 (2019).
- ¹²S. I. Rokhlin and L. Wang, “Stable recursive algorithm for elastic wave propagation in layered anisotropic media: Stiffness matrix method,” *J. Acoust. Soc. Am.* **112**(3), 822–834 (2002).
- ¹³J. F. Allard and N. Atalla, *Propagation of Sound in Porous Media: Modelling Sound Absorbing Materials 2E* (John Wiley & Sons, 2009).
- ¹⁴M. J. S. Lowe, “Matrix techniques for modeling ultrasonic waves in multilayered media,” *IEEE Trans. Ultrason. Ferroelectr. Freq. Control* **42**(4), 525 (1995).
- ¹⁵P. Agache, C. Monneur, J. L. Leveque, and J. Rigal, “Mechanical properties and Young’s modulus of human skin in vivo,” *Arch. Dermatol. Res.* **269**, 221 (1980).
- ¹⁶R. Y. Ha, K. Nojima, W. P. Adams, and S. A. Brown, “Analysis of facial skin thickness: Defining the relative thickness index,” *Plast. Reconstr. Surg.* **115**(6), 1769 (2005).
- ¹⁷S. A. Patil and J. H. L. Hansen, “The physiological microphone (PMIC): A competitive alternative for speaker assessment in stress detection and speaker verification,” *Speech Commun.* **52**(4), 327 (2010).
- ¹⁸H. Story, “An overview of the physiology, physics and modeling of the sound source for vowels,” *Acoust. Sci. Technol.* **23**(4), 195 (2002).
- ¹⁹P. Gramming, “Vocal loudness and frequency capabilities of the voice,” *J. Voice* **5**(2), 144 (1991).